ACS APPLIED BIO MATERIALS

www.acsabm.org

Article

Development of Aptamer-Functionalized Gold Nanoparticles as Probes in Point-of-Care Diagnostic Device for Rapid Detection of Multidrug-Resistant Bacteria in *Bombyx mori* L.

Rittick Mondal, Joydeep Chakraborty, Paulami Dam, Shubhajit Shaw, Debnirmalya Gangopadhyay, Yavuz Nuri Ertas,* and Amit Kumar Mandal*

Cite This: *ACS Appl. Bio Mater.* 2024, 7, 5740−5753

Read Online

ACCESS | Metrics & More | Article Recommendations

ABSTRACT: The sericulture industry suffers severe crop losses due to various silkworm diseases, necessitating the development of further technologies for rapid pathogen detection. Here, we report an all-in-one portable biosensor that combines conjugated gold nanoparticles (Au NPs) with an aptamer-based lateral flow assay (LFA) platform for the real-time analysis of *Mammaliicoccus* sp. and *Pseudomonas* sp. Our platform enables sample-to-answer naked eye detection within 5 min without any cross-reactivity with other representatives of the silkworm pathogenic bacterial group. This assay was based on the sandwich-type format using a bacteria-specific primary aptamer (Apt1) conjugated with 23 nm ± 1.27 nm Au NPs as a signal probe and another bacteria-specific secondary aptamer (Apt2)-coated nitrocellulose membrane as a capture probe. The hybridization between the signal probe and the capture probe in the presence of bacteria develops a red band in the test line, whose intensity is directly proportional to the bacterial concentration. Under the optimal experimental conditions, the visual limit of detection of the strip for *Mammaliicoccus* sp. and *Pseudomonas* sp. was 1.5×10^4 CFU/mL and 1.5×10^3 CFU/mL, respectively. Additionally, the performance of the LFA device was validated by using a colorimetric assay, and the results from the colorimetric assay are consistent with those obtained from the LFA. Our findings indicate that the developed point-of-care diagnostic device has significant potential for providing a cost-effective, scalable alternative for the rapid detection of silkworm pathogens.

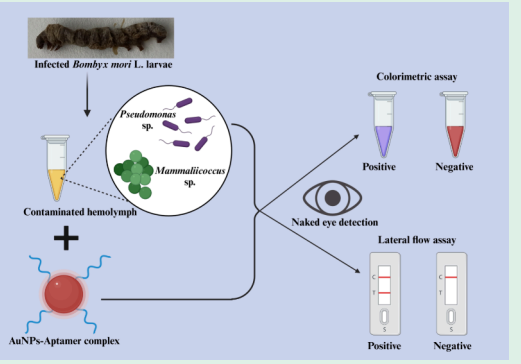

KEYWORDS: *lateral flow assay, aptamer, gold nanoparticles, point-of-care, detection, diagnostic, biosensor*

INTRODUCTION

Silk, a symbol of luxury and the supreme ruler of textiles, is in high demand in global sectors such as fashion, home furnishings, healthcare, and technology. The yield and quality of silk depend on the silkworm strain, its nutrition, climatic conditions, and silkworm health.[1] The emergence of silkworm diseases is closely related to silkworm gut microbiota.[1] Insects have symbiotic relationships with microorganisms, and their interactions with the host can vary from mutually beneficial to pathogenic.[2] The cultivation of *Bombyx mori* L. demands human intervention, which increases its vulnerability to several infectious diseases, including pebrine, flacherie, grasserie, and muscardine, leading to significant crop damage.[3] Flacherie (bacteria) and grasserie (virus) are the major killer silkworm diseases prevailing in India, causing 57.22 and 33.88% of crop losses, respectively.[4] Major silkworm pathogenic bacterial groups are *Pseudomonas* spp., *Staphylococcus* spp., *Streptococcus* spp., *Serratia* spp., *Enterococcus* spp., and *Bacillus* spp.[5,6] Additionally, the viruses that infect silkworms are *B. mori* infectious flacherie virus (BmIFV), *B. mori* densovirus (BmDNV1, BmDNV2), *B. mori* nuclear polyhedrosis virus (BmNPV), and Bm cytoplasmic polyhedrosis virus (BmCPV).[5] Furthermore, it has been confirmed that the genetic makeup of silkworms closely resembles particular genes associated with human hereditary diseases,[7] leading to a potential threat of silkworm pathogens to human health via interspecies transmission from silkworm rearing rooms.[8] Thus, it is crucial to improve silkworm rearing conditions and disease management practices. Due to the severity of silkworm pathogens, their timely recognition is crucial to preventing their transmission and carrying out precise control. The traditional method of pathogen detection opted for in silk farming mainly relies on manual identification, which has

Received: June 19, 2024
Revised: July 27, 2024
Accepted: July 30, 2024
Published: August 7, 2024

https://doi.org/10.1021/acsabm.4c00833
ACS Appl. Bio Mater. 2024, 7, 5740−5753

Table 1. Aptamers and Their Complementary DNA Sequences

target pathogens	Apt1 sequence (5′−3′)	Apt2 sequence (5′−3′)	c-DNA sequence (5′−3′)	ref
Mammaliicoccus sp. RAM2 (formerly present under the *Staphylococcus* genus)	SH-C6-TCCCTACGG CGCTAACCCCCC CAGTCCGTCCTCCC AGCCTCACACCGCC ACCGTGCTACAAC-Bio	Bio- TCCCTACGGCGCTA ACCTCCCAACCGCT CCACCCTGCCTCCG CCTCGCCACCGTGC TACAAC	Bio-GTT GTAGCACGGTGGCG GTGTGAGGCTGGGA GGACGGACTGGGG GGGTTAGCGCCGTA GGGA	31 and 32
Pseudomonas sp. RAC1	SH-C6-ATGAG AGCGTCGGTGTGGT AACTTAATCCTCTA GTTTTAATTCTAGAT ACGGCGCATGCACT CTATGTAGGAGGGT GCGGAAGTA-bio	Bio-ATGAG AGCGTCGGTGTGGT AACTAGTCTGATTT CTATTTCCTTTAATT AGTCTGCACACATT GCATTGTAGGAGGG TGCGGAAGTA	Bio-TACTTCC GCACCCTCCTACAT AGAGTGCATGCGCC GTATCTAGAATTAA AACTAGAGGATTAA GTTACCACACCGAC GCTCTCAT	33

problems like low efficiency, poor reliability, and relying on long-term professional experience that cannot accomplish the demand of the evolution and development of sericulture industries in major silk producing countries.[9] Although several molecular methods, including various PCR techniques, have been used to specifically detect silkworm pathogens, such techniques were cumbersome, requiring more time, higher cost, and trained expertise skills.[10] Therefore, an accurate, rapid, and simple method such as lateral flow assay (LFA) can offer on-site detection of such pathogens.[11] Paper-based LFA devices are superior to other standard detection platforms due to their robustness, cost-effectiveness, and user-friendly portable setup. These devices are particularly useful in biomedicine, agriculture, food, and environmental sciences for easy target detection.[12−18] These sensors are sensitive, specific, easy to use, and do not require the use of complex and expensive instrumentation.[19] More importantly, pretreatment is not required for the fluid samples, and the results can readily be interpreted with the naked eye.[20] LFA devices employ various recognition processes, such as antibody−antigen and aptamer−aptamer interactions, to detect certain analytes and provide the results to the handlers, typically through a change in color.[21] Aptamers, which are single-stranded RNA or DNA oligonucleotides, can bind to targets with high affinity and specificity, either through covalent or noncovalent methods. Due to their ability to fold specifically, aptamers have been successfully used to detect small and large molecules, such as toxins, antibiotics, and heavy metals, as well as whole cells like bacteria, even at low concentrations.[22−24] Aptamers play a significant role as a recognition element and a transducer to receive signals originated from biological and chemical specimens.[25] Moreover, in a sandwich-type dual-aptamer-based detection assay, one aptamer is employed to capture the target, while the other aptamer is utilized to generate a detection signal.[26]

Nanomaterials offer notable advances through rapid and highly sensitive pathogen probes that can be used as a rapid diagnostic approach for pathogen detection functionalized with aptamers. Gold nanoparticles (Au NPs), due to their unique optical properties, are commonly utilized to develop LFAs.[27] Generally, Au NPs are used as indicators or label substances in LFAs. Au NPs possess a high affinity for biomolecules and are highly stable due to their inert nature. Surface plasmon resonance (SPR) helps Au NPs produce a red signal that is visible to the naked eye. SPR sensors have significant advantages over other detection techniques, due to their superior sensitivity, real-time response, label-free detection, low cost, and small detection area.[28] This study reports the development of an all-in-one portable biosensor based on a conjugated Au NPs-aptamer LFA platform and colorimetric detection assay to overcome the limitations of traditional diagnostic methods for pathogen detection. Two multidrug-resistant (MDR) pathogenic bacteria, *Mammaliicoccus* sp. RAM2 and *Pseudomonas* sp. RAC1, from the hemolymph of infected silkworms were identified. *Mammaliicoccus* sp. and *Pseudomonas* sp. belong to predominant pathogenic bacterial groups responsible for infectious diseases in silkworm larvae.[29,30] Consequently, this research intended to develop a rapid detection platform for improving disease management practices. To the best of our knowledge, this is the first report of an aptamer-based LFA strip biosensor for real-time detection of pathogenic bacteria in *Bombyx mori* L.

EXPERIMENTAL SECTION

Materials and Solutions. 6-Mercapto-1-hexanol, bovine serum albumin, gold(III) chloride trihydrate ($HAucl_4{\cdot}3H_2O$), magnesium chloride, phosphate buffered saline, polyethylene glycol-20000, sodium chloride, sodium phosphate tribasic, sucrose, streptavidin, sodium saline citrate 20×, trisodium citrate ($Na_3C_6H_5O_7$), Tris (2-carboxyethyl) phosphine, Tween20, Triton X-100, and tris (hydroxymethyl) aminomethane were procured from Milipore-Sigma. Amicon Ultra Centrifugal Filter (cutoff of 30 kDa) was purchased from Millipore-Sigma. The microbial culture mediums were purchased from Himedia, India. All of the chemicals used were of analytical grade. All aqueous solutions used in the synthesis route were prepared using Milli-Q water. Aptamers and their complementary sequences were synthesized and purified through high performance liquid chromatography (HPLC) by Bioserve Biotechnologies India Pvt. Ltd. (Telangana, India) (Table 1).

Nanoparticle Synthesis. Gold nanoparticles (Au NPs) were synthesized based on the $HAuCl_4{\cdot}3H_2O$ reduction (which acts as the parent chemical) with trisodium citrate (a stabilizing agent).[32] Briefly, a reaction volume of 200 mL of $HAuCl_4{\cdot}3H_2O$ (0.25 mM) was stirred and heated at 75 °C for 15 min, and immediately, 8 mL of $Na_3C_6H_5O_7$ (w/v 1%) was added. The reaction mixture was continuously stirred and heated until a change in color of the reaction mixture from blue to wine red was observed, which indicates the formation of Au NPs. Finally, the solution was allowed to cool at room temperature, filtered through Whatman filter paper (No. 1), and stored in a dark amber bottle at 4 °C for further use.

Characterization of Au NPs. Prior to the detailed characterization of the synthesized Au NPs, a simple laser light scattering study was conducted for the confirmation of Au NP formation at the preliminary level. The synthesized Au NPs were further characterized using UV−vis spectroscopy, FT-IR, XRD, DLS, TEM, and SEM-EDX.

https://doi.org/10.1021/acsabm.4c00833
ACS Appl. Bio Mater. 2024, 7, 5740−5753

The SPR band, with λ_{max} between 500 and 550 nm of Au NPs, was verified at different time intervals using a UV−vis spectrophotometer (Labman, LMSP-UV1900) with a quartz cuvette of 1 cm optical path length in the 450−700 nm region. FT-IR (PerkinElmer Spectrum Two, part no. L1600235) was used to identify the functional groups involved in the synthesis and stabilization of the Au NPs. XRD (Rigaku Ultima IV diffractometer) analysis was employed to study the crystalline nature of the Au NPs. The zeta potential and hydrodynamic size of the synthesized Au NPs were determined by using DLS (Anton Paar, Litesizer 500). Finally, the surface morphology, shape, size, and elemental analysis of the Au NPs were investigated using both SEM (Zeiss Gemini SEM 450)-coupled EDX and TEM (Jeol, JEM-2100), as described previously.[34]

Assessing the Toxic Impact of Au NPs. *Agar Well Diffusion Method.* The zone of inhibition study was performed using the agar well diffusion method against Gram-positive *Staphylococcus aureus* MCC 2408 and Gram-negative *Pseudomonas aeruginosa* MCC 2080. The bacterial pure cultures were spread on the Mueller-Hinton agar (MHA) plates, and 8 mm diameter wells were created using a cork borer. 100 μL of synthesized Au NPs (100 μg/mL) were poured on each well and incubated overnight at 37 °C; thereafter, the zone of inhibition was measured.

Growth Kinetics Study. The mid log bacterial cells (10^6 CFU/mL) were inoculated into fresh MH broth containing 100 μg/mL Au NPs and kept for incubation at 37 °C under shaking condition (120 rpm). The bacterial growth was checked by measuring the $OD_{600\ nm}$ at different time intervals and comparing it with control sets of bacterial cells incubated without a solution of Au NPs.

SEM Analysis. SEM was used to check the alterations in bacterial cell morphology after the treatment with Au NPs. The treated *Pseudomonas aeruginosa* MCC 2080 and *Staphylococcus aureus* MCC 2408 cultures were fixed with 2.5% glutaraldehyde, dehydrated using a series of ethanol treatments, and examined under SEM (Hitachi S-3400) with an accelerating voltage in the range of 15−20 kV. Multiple fields of vision were viewed at different magnifications.[35]

Hemocompatibility of Au NPs. The hemocompatibility of the Au NPs was evaluated through a hemolytic assay.[35] A diluted solution of bovine red blood cells (RBCs, 0.2 mL) was mixed with the Au NPs at 100 ppm and incubated for 2 h at ambient temperature. The absorbance of the supernatant was measured at 541 nm via a UV−vis spectrophotometer (Labman, LMSP-UV1900), and the % hemolysis was calculated using the following equation:

$$\%\text{hemolysis} = \frac{(A_S - A_N)}{(A_P - A_N)} \times 100$$

where A_S, A_N, and A_P are the absorbances of the sample, negative control, and positive control, respectively.

Cell Line Study. The human embryonic kidney cell lines (HEK-293; ATCC accession number, CRL-1573) were used to evaluate the cytocompatibility of Au NPs. The cells were cultured in a 96-well microplate with Dulbecco's Modified Eagle Medium (Ham F-12 culture medium; DMEM/F-12) maintained at 37 °C and 5% CO_2 for 24 h, and the viability was assessed by the MTT assay, as described earlier.[36] To assess the cytotoxicity of Au NPs (from 50 to 200 ppm), 10^5 cells per well were seeded in a 96-well plate. The serially diluted Au NP solutions were applied to the surface and left to incubate for 24 h at 37 °C. 3-(4,5-Dimethylthiazol-2-yl)-2,5-diphenyltetrazolium bromide (MTT) reagent was added to each well, and the cells were incubated for 3 h. During incubation, the MTT reagent enters the mitochondria of the HEK cells and undergoes a transformation catalyzed by dehydrogenase, resulting in the formation of insoluble formazan. Next, formazan was dissolved in DMSO, and the absorbance was measured at 570 nm using a Biotek Neo 2 System microplate reader. The percentage of cell viability was calculated as

$$\text{Cell viability}\% = \frac{(\text{OD treated well} - \text{blank})}{(\text{mean OD control well} - \text{blank})} \times 100$$

DNA Fragmentation Analysis. To understand the effects of Au NPs on the structural integrity of DNA, a bacterial DNA fragmentation study was conducted. Briefly, the DNA of 16 h Au NP-treated *Pseudomonas aeruginosa* MCC 2080 and *Staphylococcus aureus* MCC 2408 was extracted using the standard phenol−chloroform method.[37] As a negative control, cells were incubated without Au NPs for the same period to compare our results. Both the DNA samples that underwent treatment and those that did not (control) were subjected to electrophoresis. Afterward, they were stained with ethidium bromide, observed under UV light, and captured using a Bio-Rad ChemiDoc MP Imager system (model no. 12003154).

In Vivo Toxicity Evaluation of Au NPs on B. mori. The cytotoxicity of the synthesized Au NPs was checked through monitoring the *B. mori* rearing parameters such as larval length weight and survivability, cocoon weight, shell weight, cocoon shell percentage, average filament length, denier, and renditta using the protocols described previously.[38]

Isolation of Pathogenic Bacterial Strain from Infected Silkworm. Infected Nistari races of *Bombyx mori* L. larvae (5th instar) were collected from the silkworm rearing house of Raiganj University, India. The collected larvae were washed with ethanol (70%), surface sterilized with sodium hypochlorite (5%) for 5 min, and finally rinsed three times with sterile deionized water. Infected larvae (3rd day of fifth instar) ruptured in the first abdominal leg using a sterile superfine 31G short needle to collect hemolymph in a prechilled microtube. Thereafter, the collected hemolymph was spread on mannitol salt agar and cetrimide agar media plates and incubated overnight at 37 °C. Following incubation, individual colonies were selected and moved to fresh medium in order to achieve pure colonies.[39] Moreover, the isolates were stored at −70 °C in 20% glycerol for future use.

Vitek-2 Compact Automated System-Based Bacterial Biochemical Characterization. The bacterially pure cultures (RAM2 and RAC1) were placed in separate polystyrene tubes containing 3 mL of a saline solution (0.45%). The suspensions were vigorously vortexed to achieve uniform homogenization, and the turbidity of the solution was calibrated using a VITEK Densichek (BioMérieux) instrument to correspond to the McFarland 0.5−0.63 standard. Subsequently, the VITEK-2 identification cards were put into polystyrene tubes, and the results were generated by the system.

Phylogenetic Analysis of Silkworm Infecting Bacteria. Genomic DNA of the freshly grown isolates (RAM2 and RAC1) was extracted using the standard phenol−chloroform method, as described earlier.[37] The 16S rDNA was amplified using the universal primers 27F, 704F, and 907R[40,41] and sequenced using the Sanger sequencing technique. After this, both strands of sequenced nucleotides were aligned using the BioEdit program to retrieve the 16S rDNA sequence of the isolates, and the sequences were submitted to the EZBioCloud server (https://www.ezbiocloud.net/) to identify the closest type strains. All of the closest type strains for both of the isolated strains were downloaded to obtain multiple sequence alignment with the ClustalW program using MEGA11 software. The neighbor joining (NJ) method was used to generate phylogenetic trees with evolutionary distances computed using the Kimura 2 parameter model. The bootstrap analysis was performed on both phylogenetic trees, with 1000 resampling iterations, to validate each clade of the phylogenetic tree.[34] The NCBI accession numbers for the 16S rDNA sequences of the selected strains RAM2 and RAC1 are OQ629874 and OQ629864, respectively.

SEM Analysis of Silkworm Infecting Bacteria. The SEM micrographs of freshly grown isolates (RAM2 and RAC1) were captured following the protocol described previously in the earlier section.[35]

Antimicrobial Susceptibility Testing. A Kirby−Bauer disc diffusion test was conducted to examine the antibiogram profiles of the isolated RAM2 and RAC1.[39] Hexa disks of various classes of antibiotics were purchased from HiMedia Laboratories Pvt. Ltd., India. The freshly grown culture of isolated strains was spread, and the discs were placed on top of the Mueller−Hinton agar plates and incubated overnight at 37 °C. The isolated bacteria were classified as sensitive to drugs that formed halo inhibition zones, whereas those

https://doi.org/10.1021/acsabm.4c00833
ACS Appl. Bio Mater. 2024, 7, 5740−5753

Scheme 1. Schematic Illustration of the (a) Synthesis Route of Au NPs and (b) the LFA Test Strip Biosensor for the Rapid Detection of Targeted Silkworm Pathogen

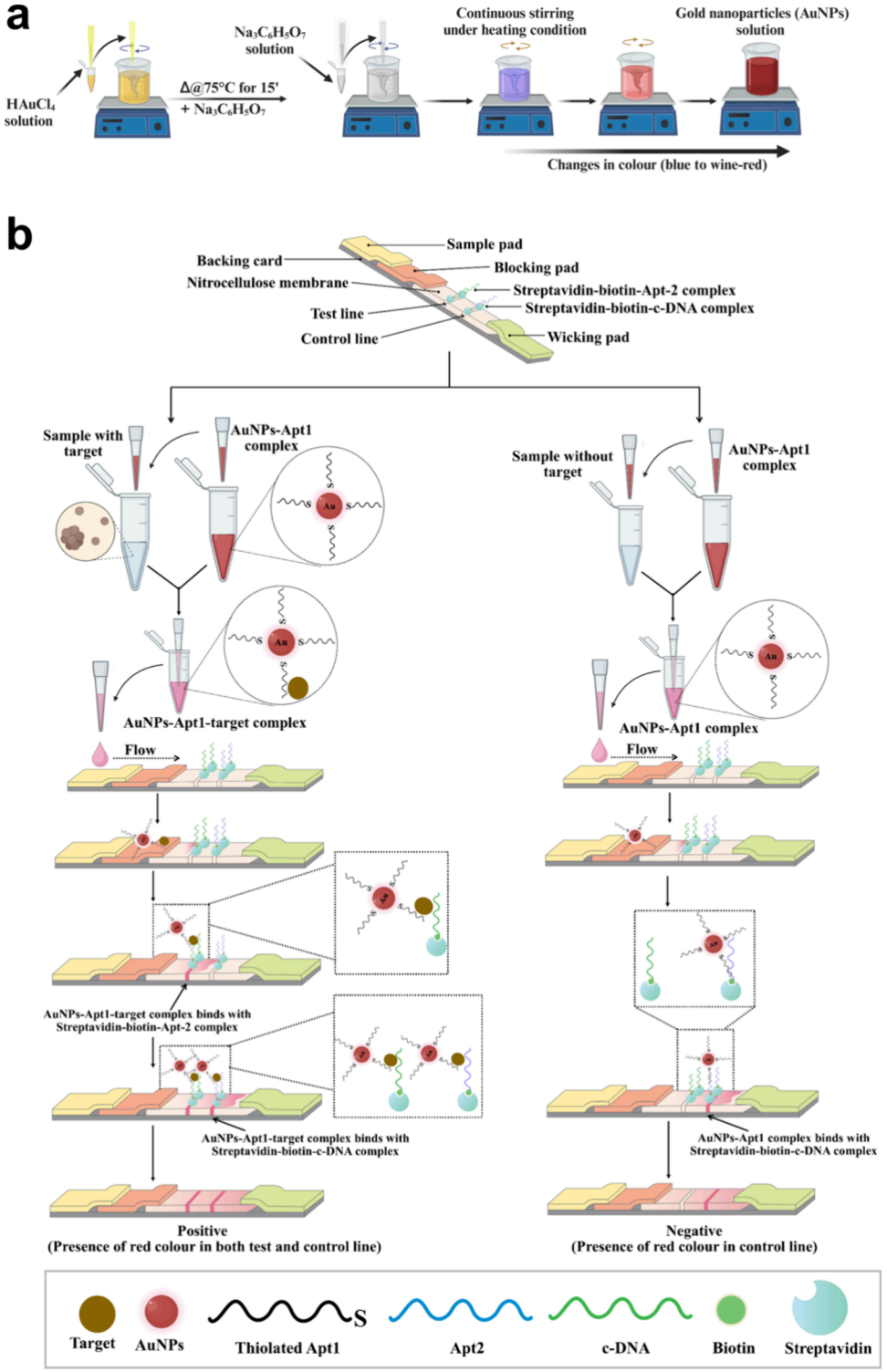

that did not form halo inhibition zones were classified as resistant to those antibiotics.

Development of LFA Test Strip Biosensor for the Detection of *Pseudomonas* sp. RAC1 and *Mammaliicoccus* sp. RAM2. *Preparation of Au NPs−Apt1 Conjugate.* The Au NPs−aptamer conjugates were prepared through a series of steps that are predicated upon the interaction between thiolated DNA strands and Au NPs, facilitated by a gold−sulfur reaction. Briefly, 5 μL of thiolated aptamer (100 μM; Apt1) was folded into its tertiary structure by incubating it with 45 μL of folding buffer comprising 1 mM $MgCl_2$ and 1× PBS (pH 7.4) at room temperature. Subsequently, the solution underwent a controlled heat treatment at 90 °C for 5 min, followed by a gradual cooling to room temperature over approximately 15 min. After being activated with 2 μL of TCEP (20 mM), 50 μL of thiol aptamer (10 μM) underwent incubation at room temperature for 1 h. Subsequently, 40 μL of Au NPs (with an optical density of 7.5) and 2 μL of the activated aptamer were mixed and left to incubate in a dark, ambient environment for 8 h. Sodium chloride (1 M) was

https://doi.org/10.1021/acsabm.4c00833
ACS Appl. Bio Mater. 2024, 7, 5740−5753

administered incrementally to the mixture until it reached a final concentration of 200 mM NaCl, which served to enhance DNA loading onto the surface of Au NPs. After refrigeration overnight, unconjugated thiol-aptamers were removed by centrifugation (12,000 rpm for 10 min) and washed three times with nanofiltration water. To block unoccupied sites on the Au NPs' surface, 2 μL of MCH (28 μM) was added to 50 μL of conjugated Au NPs−aptamer and incubated for 1 h before washing off the excess MCH. This process ensured the successful preparation of Au NPs−Apt1 conjugates with minimal unbound aptamers. Moreover, the amount of Apt1 in Au NPs−Apt1 conjugates was estimated by measuring the absorbance at 260 nm using Multimode Microplate Reader, BioTek Synergy H1m (USA).

Preparation of Streptavidin−Biotin−DNA Conjugates. The formulation of the test line solution commenced with the addition of 69 μL of biotin−Apt2 (10 μM) and 23 μL of streptavidin (1 mg/mL). After a 1 h incubation period at room temperature, the resultant mixture underwent centrifugation at 6000 rpm utilizing a centrifugal filter (with a cutoff of 30 kDa, Millipore) for a duration of 20 min to expel surplus aptamers. PBS was then incrementally introduced into the solution to reinstate its initial volume prior to the centrifugation process. The preparation of the control line solution entailed the addition of an equimolar volume of streptavidin (1 mg/mL) to c-DNA (10 μM). Following a 1 h incubation period under ambient conditions, the solution was augmented with 20 × 12.5% SSC.

Assembly of Aptamer-Based LFA Strips and Sample Preparation. The test strip for bacteria consists of four components: sample pad, blocking agent pad, nitrocellulose (NC) membrane (Cat. No.: LJDFXXX060 × 260X; Type: 70CNPH-N-SS40-L2-P25), and wicking pad (Cat. No.: P080XXX022 × 260X; Type: AP080). All four parts were mounted on an adhesive backing card with a 2 mm overlap to facilitate liquid flow between the membrane and the pads. The assembled components were cut into 3 mm wide individual test strips using a programmable strip cutter (Model: M-70, Advanced Sensors Systems Pvt. Ltd., Haryana, India). Streptavidin−biotin−Apt2-complex (30 μL) and streptavidin−biotin−c-DNA complex (30 μL) were dispensed on the NC membrane using a printer (Model: LPM-02, Advanced Sensors Systems Pvt. Ltd., Haryana, India) dispensing machine, which formed the test and control lines, respectively. These lines were ∼3 mm apart.

Sample pads (Cat. No.: PGF4D35014 × 260X; Type: GFB-R4) soaked in a buffer solution (0.15 mM NaCl, 0.05 M Tris, and 0.25% Triton X-100 (pH 8) and blocking pads (Cat. No.: PTR5XXX070 × 260X; Type: PT-R5) were soaked in a different buffer (5% BSA, 20 mM Na_3PO_4, 10% sucrose, and finally 0.25% Tween20). Both pads were soaked for 30 min in their respective buffers and then dried at 45 °C for 90 min. The inclusion of a sample buffer in the sample pad facilitates the movement of the dispensed solution into the membrane. Blocking agents were employed to diminish the nonspecific binding of the aptamer to the NC membrane. In order to prevent the impact of moisture on the rate of flow, the test strips were subjected to a drying process at 60 °C for 10 min. Subsequently, they were stored at room temperature in boxes that were equipped with silica desiccant to absorb any remaining moisture.

Bacterial Culture Preparation. The tested bacterial strains were grown and quantified by following standard protocols. In short, all strains were grown overnight in LB medium at 37 °C until reaching an OD_{600} of 1.0. The cultures were then centrifuged, washed, and suspended in sterile 1× PBS (pH 7.4). The bacterial quantities were assessed using the viable plate count method.[32]

Assay Procedures. To conduct the biosensing assay, the tested bacterial cultures were diluted with sterile 1× PBS (pH 7.4) to obtain different test solution concentrations. Portions of 100 μL of this bacterial suspension were mixed with 5 μL of a conjugated Au NPs-Apt1 solution and left to incubate for 10 min at room temperature in the dark. Subsequently, 80 μL of this mixture was applied to the sample pad of the aptamer-based lateral flow strip, allowing it to migrate along the strip. The test and control lines were observed visually within 10 min (Scheme 1).[42]

Real Sample Analysis. The effectiveness of the LFA test strip biosensor detection for *Pseudomonas* sp. RAC1 and *Mammaliicoccus* sp. RAM2 was evaluated using infected silkworm hemolymph. Infected fifth instar larvae of *Bombyx mori* L. were collected from different sericulture practiced districts of West Bengal, India. These larvae were treated with 70% ethyl alcohol, followed by surface sterilization using 5% sodium hypochlorite for 5 min and then rinsed three times with sterile deionized water. Hemolymph was extracted as described in an earlier section.[39] The infected hemolymph samples (100 μL) were mixed with sterile 1× PBS (300 μL), and 80 μL of these mixtures were utilized for assessment, following our standardized assay procedure.[32]

Colorimetric Assay. The colorimetric assay-based detection of *Pseudomonas* sp. RAC1 and *Mammaliicoccus* sp. RAM2 was performed at ambient temperature using the LOD value (1.5×10^3 CFU/mL for *Pseudomonas* sp. RAC1 and 1.5×10^4 CFU/mL for *Mammaliicoccus* sp. RAM2), which was acquired from our LFA. For each detection measurement, 10 μL of Apt1 (30 μM) was mixed with 10 μL of c-DNA (30 μM) in the presence of 30 μL of nuclease-free deionized water and incubated for 1 h. Afterward, the mixture was added to the Au NP solution (950 μL) and left undisturbed for 1 h. A volume of 50 μL of both bacterial concentrations was mixed separately with 100 μL of their respective dsDNA (Apt1−cDNA mixture)−Au NP solution and incubated for 35 min. Thereafter, 6 μL of a NaCl (1 M) solution was added to the mixture and incubated for 5 min. The absorption spectra were recorded using a UV−vis spectrometer in the range of 400−700 nm, and changes in the solution color were observed. Furthermore, the specificity of the colorimetric assay toward *Pseudomonas* sp. RAC1 or *Mammaliicoccus* sp. RAM2 was investigated using nontargeted bacterial strains, including *Staphylococcus aureus* MCC 2408, *Serratia marcescens* ATCC 8100, or *Pseudomonas aeruginosa* MCC 2080, and *Streptococcus mutans* MTCC 497, respectively.

RESULTS AND DISCUSSION

Synthesis and Characterization of Au NPs. Au NPs were formed successfully, as indicated by changes in the color of the solution to wine red. Furthermore, the Au NP formation was confirmed using laser light-mediated Tyndall scattering (Figure 1a).

Ultraviolet−visible (UV−vis) spectra showed an SPR band centered at ∼520 nm, which is the typical characteristic of Au NPs, clearly indicating NP formation. This is due to the excitation of the SPR effect and the reduction of $AuCl_4^-$ ions (Figure 1b). The blue shift as revealed in the UV−vis spectra indicates a decrease in particle size or surface dissolution of gold atoms.

Fourier transform infrared spectroscopy (FT-IR) was utilized to identify the major functional groups responsible for Au NP formation. The FT-IR spectrum exhibited a peak around 3609.88 cm^{-1} assigned to −O−H. The two peaks around 2922.95 and 1715.60 cm^{-1} were associated with −C−H and −C=O stretching vibrations, respectively, which indicates the formation of citrate-stabilized Au NPs (Figure 2a). These findings coincided with the previously reported study.[43] The crystalline structure of Au NPs was determined by X-ray diffraction (XRD) analysis. The XRD peaks of intensity at the 2θ values of 38.29°, 44.47°, 64.66°, and 77.59°, corresponding to the (111), (200), (220), and (311) planes, reveal the face-centered cubic (fcc) nature of the synthesized Au NPs (Figure 2b). Hydrodynamic diameter is a significant parameter for the morphological behavior of colloidal particles. The synthesized Au NPs showed a peak zeta potential of −25.5 mV with a hydrodynamic diameter of 26.5 nm (Figure 2c,d). Our results revealed that the synthesized Au NPs were quite stable. The zeta potential is predictive of colloidal stability,

https://doi.org/10.1021/acsabm.4c00833
ACS Appl. Bio Mater. 2024, 7, 5740−5753

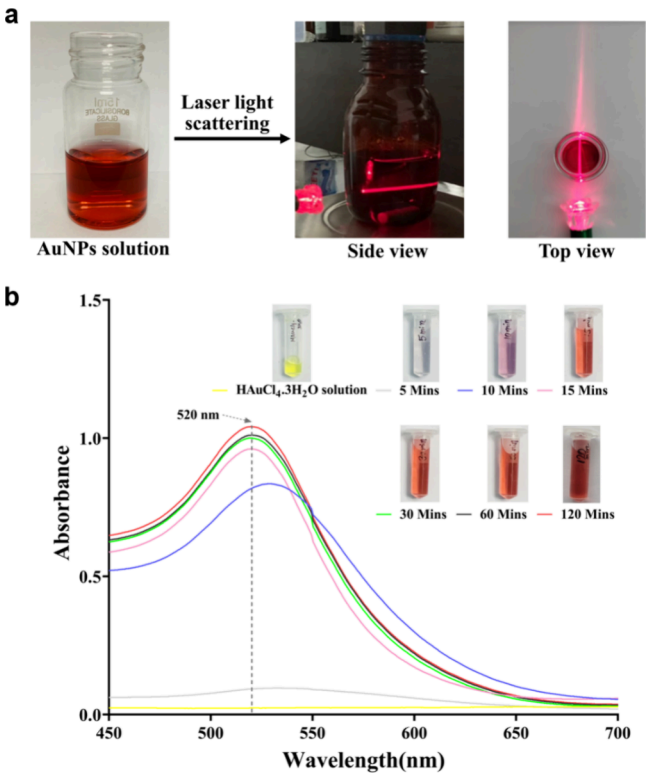

Figure 1. (a) Confirmation of the Au NP formation via laser light scattering: laser light passes through Au NPs due to Tyndall scattering, which confirms the formation of Au NPs. (b) UV−vis spectra of synthesized Au NPs showing SPR band around 520 nm.

where values >+25 mV or <−25 mV typically have a high degree of stability, which supports our claim.[44] The distribution of large zeta potential for the synthesized citrate capped Au NPs could be explained by the polydispersity in size. Additionally, variation in the amount of citrate adsorbed on the surface of individual Au NPs can also lead to differences in surface charge density and zeta potential.[45]

SEM and TEM revealed the nearly spherical morphology of Au NPs (Figure 3a,b). The lattice constant was measured as 0.235 nm from TEM photograph, confirming the crystalline nature of the NPs[46] (Figure 3c). An average particle size of 23 nm ± 1.27 nm was determined through the histogram of the particle size distribution (Figure 3d). The energy-dispersive X-ray (EDX) spectrum of Au NPs exhibited strong peaks corresponding to Au approximately at 2.2, 9.7, and 11.5 keV, as displayed in Figure 3e, which is typical for the absorption of metallic Au nano crystallites due to SPR, which were concomitant with previously reported results.[47] The elemental mapping analysis of the Au NPs exhibited a wide distribution of metallic gold (Figure 3e inset).

Assessing the Toxic Impact of Au NPs. *Impact of Au NPs on Bacterial Growth Kinetics and Morphology.* The synthesized Au NPs did not show any significant toxicity against the tested microorganisms (*Pseudomonas aeruginosa* MCC 2080 and *Staphylococcus aureus* MCC 2408) as there was no zone of inhibition observed. Figure 4a shows that synthesized Au NPs did not have any growth inhibition effects on any of the tested bacterial cells. Au NPs were reported to reduce bacterial cell division time with a 2-fold increase in bacterial cell density without damaging its DNA.[48] SEM micrographs revealed that there were no structural changes in the bacterial cells after treatment with Au NPs, and the cell morphology was almost the same as that observed for the control (without any NP treatment) (Figure 4b).

In Vitro and In Vivo Biocompatibility Analysis of Au NPs. Hemolytic Assay. A hemolysis assay is a basic experiment to ascertain the hemocompatibility of any nanoparticles. Our results revealed that 100 ppm of Au NPs exhibited 1.03% hemolysis (Figure 5a). NPs exhibiting <5% hemolysis are considered hemocompatible.[49,50] A diluted RBC suspension

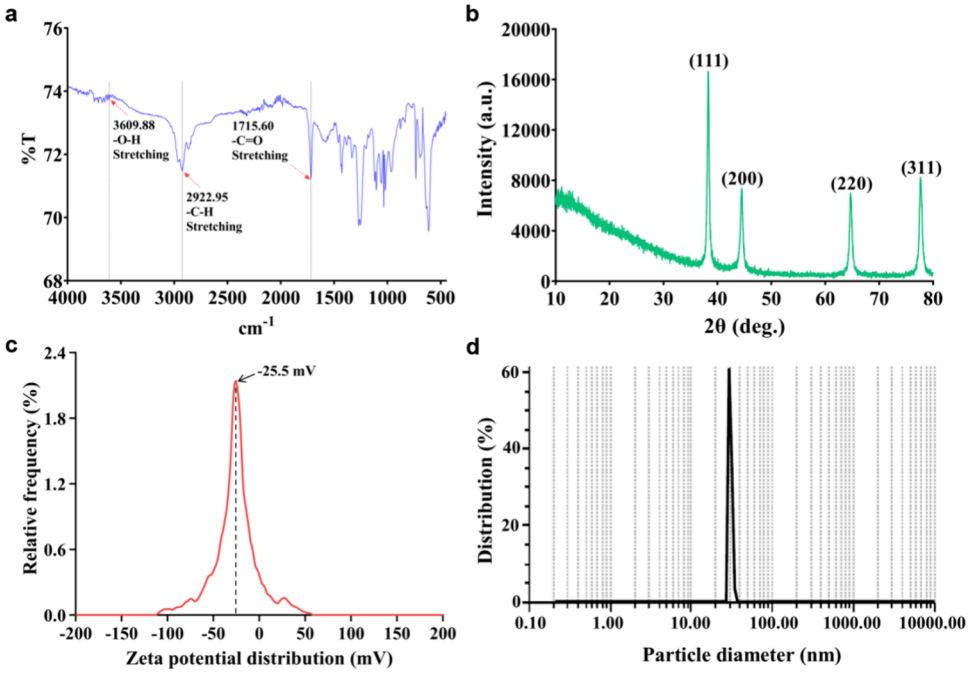

Figure 2. (a) FT-IR spectrum of the synthesized Au NPs. (b) XRD spectrum of Au NPs. (c) Zeta potential of Au NPs. (d) Dynamic light scattering plot for distribution of hydrodynamic diameter of Au NPs.

https://doi.org/10.1021/acsabm.4c00833
ACS Appl. Bio Mater. 2024, 7, 5740−5753

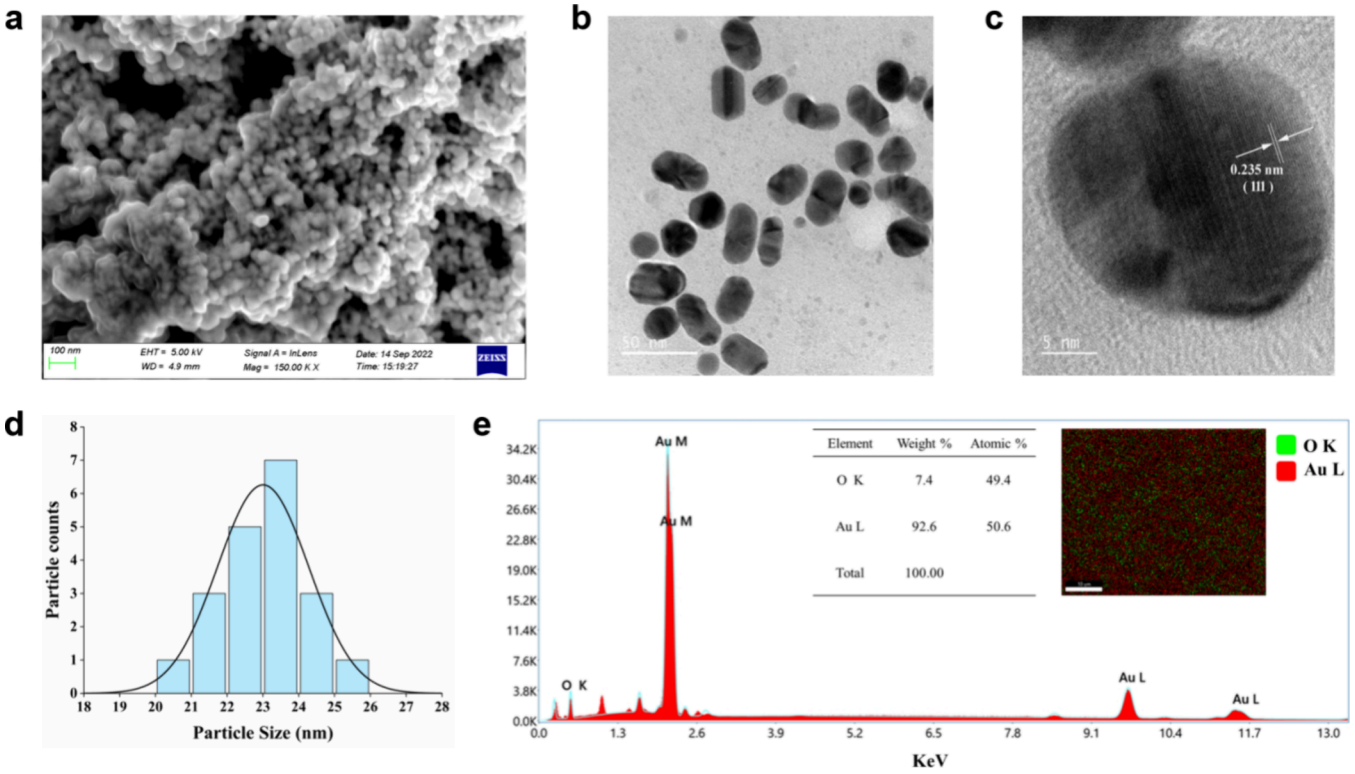

Figure 3. (a) SEM micrograph of synthesized Au NPs. (b) TEM micrograph of Au NPs. (c) Lattice constant of Au NPs. (d) Particle size distribution of synthesized Au NPs. (e) EDX spectra exhibited strong signal of Au, and the inset shows distribution of gold in elemental mapping.

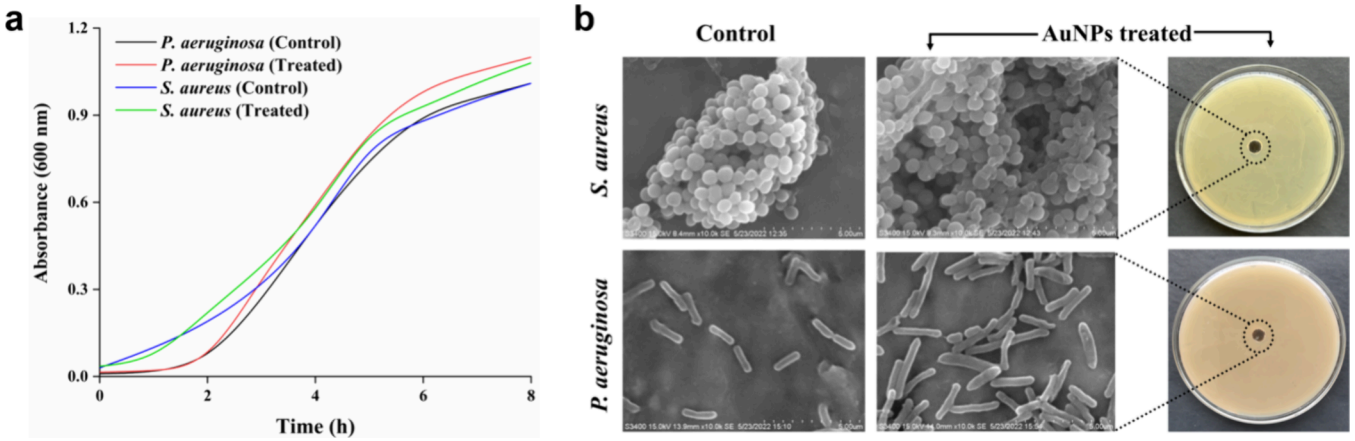

Figure 4. (a) Growth kinetics and (b) SEM micrograph of *Pseudomonas aeruginosa* MCC 2080 and *Staphylococcus aureus* MCC 2408 in the presence (treated) and absence (control) of Au NPs.

mixed with 0.8 mL of PBS and 0.8 mL of double-distilled water was used as negative and positive controls, respectively.

Cytocompatibility Assay. MTT tests were performed to assess the impact of Au NPs on the viability of human embryonic kidney cells (HEK-293). The experiments included various doses of Au NPs, ranging from 50 to 200 ppm (Figure 5b). The test quantifies the cellular energy capacity by evaluating the functionality of the mitochondrial respiration system. The process involves the use of MTT, a yellow dye, which undergoes a color change to blue upon reduction by oxidoreductase in the presence of NADPH. The observed alteration occurs only in living cells; hence, the amount of blue formazan generated is proportional to the number of viable cells. In our case, up to 200 ppm of Au NPs, there was no significant reduction in cell viability compared with the control, indicating the biocompatibility of Au NPs.

DNA Fragmentation Study. DNA gel electrophoresis was used to study whether the synthesized Au NPs induce DNA fragmentation. Bacterial cells were treated with 100 ppm of Au NPs for 16 h, and then, genomic DNA was isolated. DNA fragmentation was documented using 1% agarose gel electrophoresis (Figure 5c,d). According to the comparison with the not-treated control set, 100 ppm Au NPs did not induce any DNA fragmentation in both treated cells, suggesting their biocompatible nature and thus being suitable for biomedical applications.[51]

In Vivo Toxicity Evaluation of Au NPs on B. mori. For a better evaluation of the safety and toxicity of the Au NPs and the absence of biokinetics in the in vitro system, an in vivo

https://doi.org/10.1021/acsabm.4c00833
ACS Appl. Bio Mater. 2024, 7, 5740−5753

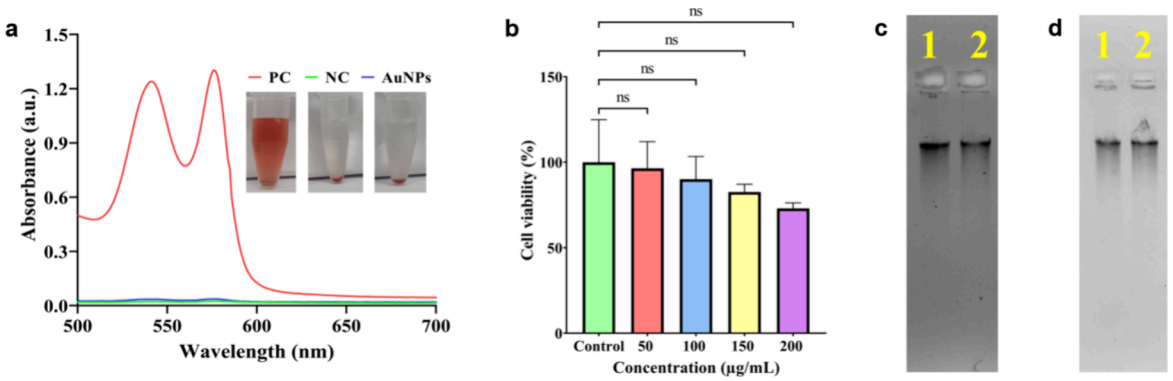

Figure 5. (a) Hemocompatibility assay of synthesized Au NPs. (b) Cytocompatibility assay of Au NPs. DNA fragmentation assay of (c) *Staphylococcus aureus* MCC 2408 and (d) *Pseudomonas aeruginosa* MCC 2080 cells (Lane 1: control; Lane 2: Au NP treated).

Table 2. Efficacy of Varied Concentration of Au NPs on Rearing and Reeling Performances of *B. mori*[a]

	treatments					
	control		Au NPs (50 ppm)		Au NPs (100 ppm)	
particulars	Nistari[b]	Nistari × NB_4D_2[c]	Nistari[b]	Nistari × NB_4D_2[c]	Nistari[b]	Nistari × NB_4D_2[c]
larval weight (gm)	2.73 ± 0.02	3.36 ± 0.02	2.93 ± 0.03 (7.32)	3.47 ± 0.04 (3.27)	2.96 ± 0.03 (8.42)	3.49 ± 0.02 (3.86)
larval survivability (%)	90.88 ± 1.15	92.60 ± 1.15	91.26 ± 1.15 (0.41)	93.12 ± 1.15 (0.56)	93.31 ± 1.15 (2.67)	95.24 ± 2 (2.85)
cocoon weight (gm)	1.16 ± 0.01	1.48 ± 0.08	1.32 ± 0.04 (13.79)	1.62 ± 0.08 (9.45)	1.56 ± 0.05 (34.48)	1.85 ± 0.08 (25.00)
shell weight (gm)	0.160 ± 0.002	0.239 ± 0.002	0.185 ± 0.005 (15.62)	0.267 ± 0.004 (11.71)	0.223 ± 0.045(39.37)	0.317 ± 0.003(32.63)
cocoon shell (%)	13.79 ± 0.44	16.14 ± 0.14	13.99 ± 0.31 (1.45)	16.51 ± 0.05 (2.29)	14.32 ± 0.31 (3.84)	17.15 ± 0.05 (6.25)
filament length (m)	433 ± 6	815 ± 2.51	463 ± 9.8 (6.92)	848 ± 3.51 (4.04)	485 ± 7 (12.00)	906 ± 2.51(11.16)
denier (d)	1.77 ± 0.02	1.84 ± 0.01	1.75 ± 0.02 (−1.12)	1.82 ± 0.005 (−1.08)	1.72 ± 0.04 (−2.82)	1.81 ± 0.005(−1.63)
renditta	13.16 ± 0.06	9.55 ± 0.015	13.05 ± 0.07 (−0.83)	9.00 ± 0.18(−5.75)	12.95 ± 0.07 (−1.59)	8.90 ± 0.05(−6.80)

[a]Data represent mean ± SD of three replicates. [b]Nistari an indigenous polyvoltine (pure) silkworm breeds. [c]Nistari × NB4D2 a crossbred between polyvoltine and bivoltine silkworm breeds; data in parentheses indicate percent improvement compared to the control.

study was performed using *B. mori* L. as an animal model. Silkworm larvae were fed with the synthesized Au NPs starting from the fifth instar, and their survival, larval weight, cocoon weight, shell weight, cocoon shell percentage, filament length, denier, and renditta were measured and percent improvement was calculated with respect to the control. We found that at 50 and 100 ppm, Au NPs enhanced both rearing and reeling performance of *B. mori* without any adverse side effects as compared to the control (Table 2).

Biochemical Characterization, Molecular Identification, and SEM Analysis of Pathogenic Bacterial Strains of Infected Silkworm. The biochemical characterization of RAM2 and RAC1 was performed using VITEK-2 automated technology for the identification of individual species or bacterial groups. Based on the biochemical characteristics, the Vitek-2 automated system identified the strain RAM2 as *Staphylococcus sciuri* (now known as *Mammaliicoccus sciuri*[31]) with a 99% probability. However, a low-discrimination identification was observed between three microorganisms (*Pseudomonas fluorescens*, *Pseudomonas stutzeri*, and *Pandoraea* spp.) in the case of RAC1. An earlier study reported that low-discrimination identifications were frequent in Vitek-2 automated system-based identification.[52] All of the low-discrimination identifications were further resolved by performing 16s-rDNA-based phylogenetic identification. The phylogenetic tree analysis revealed that isolated bacterial strains, i.e., RAM2 (NCBI accession no. OQ629874), show 99.86% similarity with *Mammaliicoccus sciuri* DSM 20345 (2 nt differences) and RAC1 (NCBI accession no. OQ629864) shows 99.58% similarity with *Pseudomonas fulva* NBRC 16637 (6 nt differences) (Figure 6a,b). Furthermore, SEM revealed that the isolated strain, *Mammaliicoccus* sp. RAM2 was round-shaped, with an average diameter of 0.76 μm and *Pseudomonas* sp. RAC1 was rod-shaped, with an average diameter of 1.24 μm (Figure 6c,d).

Antibiogram Profiling. The sericulture industry often employs antibiotics to improve cocoon and raw silk output, ensuring the health- and disease-free status of the silkworms. This opens Pandora's Box of antibiotic abuse and overuse[8] and necessitates understanding the antibiotic resistance pattern in silkworm pathogens. The antibiogram study of *Mammaliicoccus* sp. RAM2 and *Pseudomonas* sp. RAC1[39] showed that both the tested strains were resistant to different classes of antibiotics, including cell wall inhibitors, nucleic acid synthesis inhibitors, and protein synthesis inhibitors, and thus depicted as multidrug-resistant MDR (Table 3). Enlarging the toolbox against MDR strains, we have developed a strategy to identify such MDR strains through a sandwich-type dual-aptamer-functionalized Au NPs-based LFA test strip biosensor rapid detection kit.

Sensitivity and Specificity of the LFA Test Strip Biosensor. Au NPs-thiol modified aptamer conjugation has opened diverse avenues and is frequently utilized for biosensing applications due to its high stability and specificity toward their target. A stable conjugation is formed between the gold surface and the sulfur atoms of the thiolated aptamer via

https://doi.org/10.1021/acsabm.4c00833
ACS Appl. Bio Mater. 2024, 7, 5740−5753

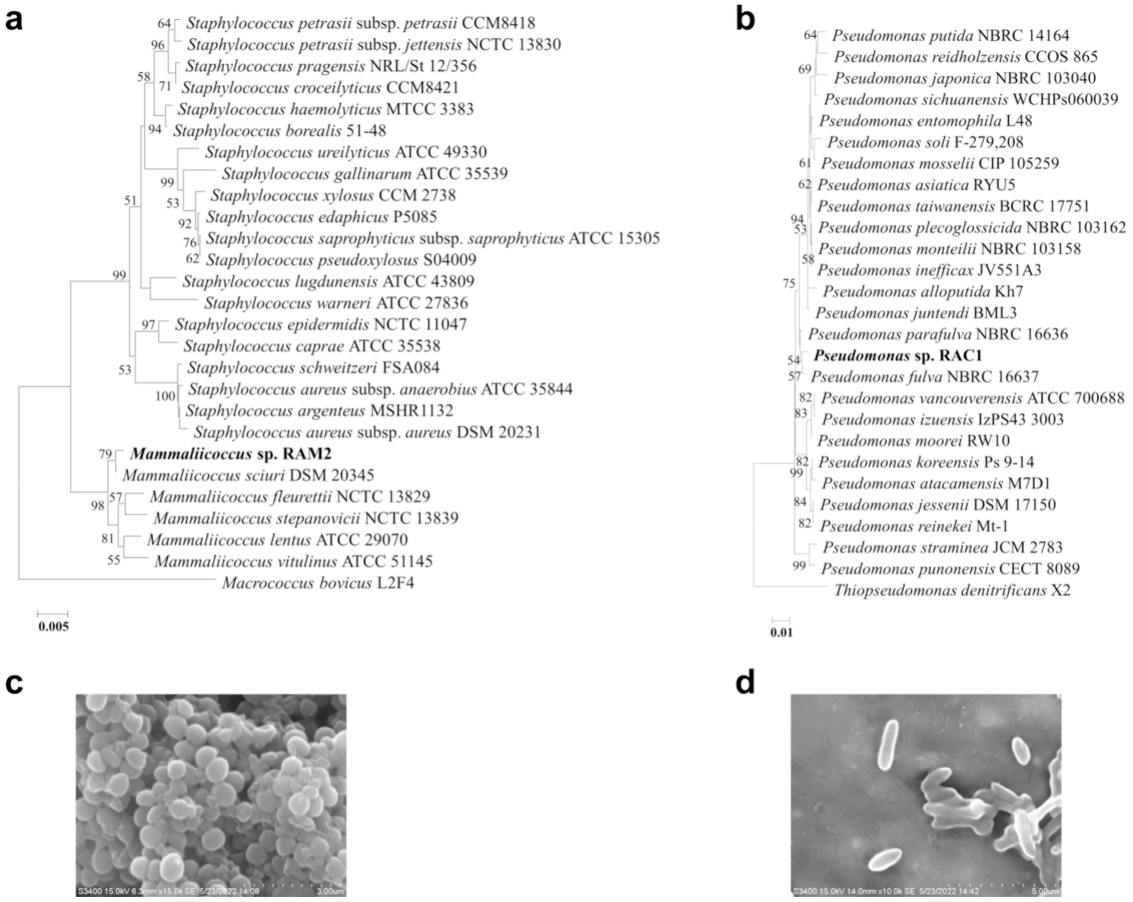

Figure 6. Neighbor joining phylogenetic tree of (a) isolate RAM2 and (b) RAC1 based on 16S rDNA linear sequence. Only >50% bootstrap value is shown at branch node from 1000 replicates. SEM micrograph of (c) *Mammaliicoccus* sp. RAM2 and (d) *Pseudomonas* sp. RAC1.

Table 3. Antibiotics Resistance Profiling of the *Mammaliicoccus* sp. RAM2 and *Pseudomonas* sp. RAC1

name of the microorganisms	name of the resistant antibiotics
Mammaliicoccus sp. RAM2	Fusidic acid, Cloxacillin, Nalidixic acid
Pseudomonas sp. RAC1	Ampicillin, Amoxyclav, Penicillin-G, Vancomycin, Teicoplanin, Cefoxitin, Oxacillin, Cephalothin, Cloxacillin, Methicillin, Fusidic acid, Linezolid, Lincomycin, Rifampicin, Nitrofurantoin, Co-Trimoxazole, Sulphatriad

the gold−sulfur interactions. The aptamer coating on Au NPs can prevent the aggregation of the NPs via electrostatic repulsion, owing to the presence of phosphate groups present on the aptamers at high salt concentrations.[53]

In the designed LFA test strip biosensor, the sample containing the Au NPs-Apt1 (bacteria-specific) target complex migrates through the LFA strip. As it passes through, it gets captured by the bacteria-specific second aptamer (Apt2) fixed on the test line, resulting in a visible red band. Any remaining Au NPs-Apt1 complex moves further to the control line, where it binds with the complementary DNA (c-DNA) of Apt1, creating another red band. If there is no target present, then only the control line shows a red band. This ensures the reliability of the assay regardless of whether the target is present or not. Our studies revealed that the concentration of Apt1 for both *Pseudomonas* sp. RAC1 and *Mammaliicoccus* sp. RAM2 in the Au NPs-Apt1 conjugates was found to be 971.73 ng/μL and 892.6 ng/μL, respectively. However, further research is needed to detect the exact amount of captured-Apt1 per Au NPs.

To test the sensitivity, we examined various concentrations of *Pseudomonas* sp. RAC1 and *Mammaliicoccus* sp. RAM2 (from 1.5×10^8 to 1.5×10^1 CFU/mL) under optimal experimental conditions. We visually assessed the test line for target detection. The color intensity of the test line gradually decreased as the concentration of the target pathogens decreased in the detection solution. Our study demonstrated that the test lines disappeared after a concentration of 1.5×10^3 CFU/mL for *Pseudomonas* sp. RAC1 and 1.5×10^4 CFU/mL for *Mammaliicoccus* sp. RAM2. Thus, we estimated the visual limit of detection (LOD) of this LFA test strip biosensor to be 1.5×10^3 CFU/mL for RAC1 and 1.5×10^4 CFU/mL for RAM2 (Figure 7a). Furthermore, our results were also compared with previously reported related assays (Table 4) to gain a better understanding of its sensitivity.

Additionally, the LFA test strip biosensor was designed for *Pseudomonas* sp. RAC1 and *Mammaliicoccus* sp. RAM2 were examined vis-à-vis an array of other bacterial strains (as a representative of the silkworm pathogenic bacterial group) to ascertain cross-reactivity and specificity. The study involved six different quality control bacterial strains, including *Streptococcus mutans* MTCC 497, *Pseudomonas aeruginosa* MCC 2080, *Bacillus cereus* ATCC 11778, *Staphylococcus aureus* MCC 2408, *Serratia marcescens* ATCC 8100, and *Enterococcus faecalis* MCC 2409. Each tested bacterium was standardized to a concentration of 1.5×10^8 CFU/mL. The *Pseudomonas* sp.

https://doi.org/10.1021/acsabm.4c00833
ACS Appl. Bio Mater. 2024, 7, 5740−5753

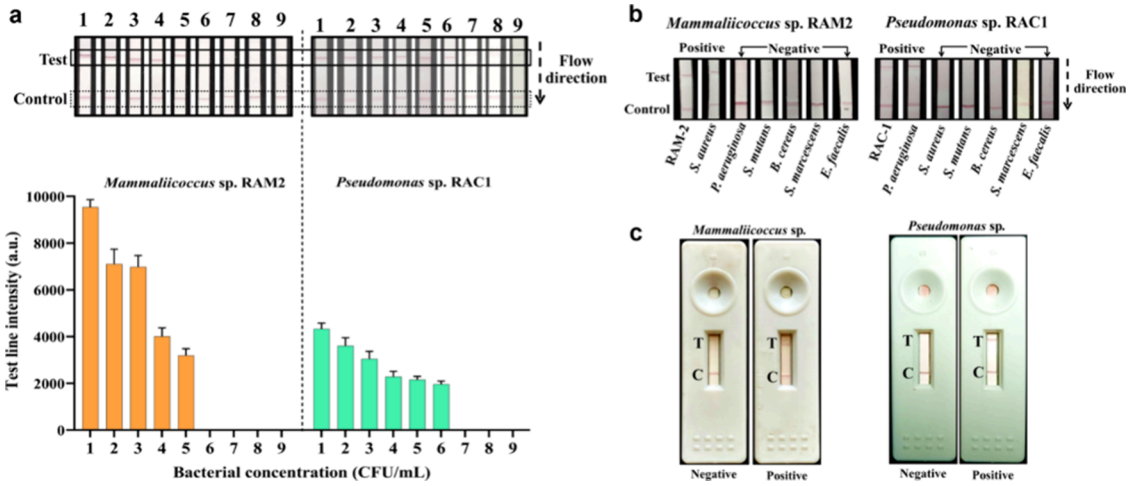

Figure 7. (a) Sensitivity of LFA test strip biosensor. Visual observation of the effect of bacterial concentration on color intensity of the test line and LOD for *Mammaliicoccus* sp. RAM2 and *Pseudomonas* sp. RAC1, and the peak areas of test line signal intensity were calculated by ImageJ analysis. Graph shows the mean ± SD of three independent measurements (1: 1.5×10^8 CFU/mL; 2: 1.5×10^7 CFU/mL; 3: 1.5×10^6 CFU/mL; 4: 1.5×10^5 CFU/mL; 5: 1.5×10^4 CFU/mL; 6: 1.5×10^3 CFU/mL; 7: 1.5×10^2 CFU/mL; 8: 1.5×10^1 CFU/mL; and 9: control). (b) Specific detection of *Mammaliicoccus* sp. and *Pseudomonas* sp. in the presence of other bacteria using the LFA test strip biosensor. (c) Detection of *Mammaliicoccus* sp. and *Pseudomonas* sp. in infected silkworm hemolymph sample using the LFA test strip biosensor.

Table 4. Comparison of Detection Performance between Existing Detection Methods and the Proposed Method in This Study

strategy	recognition molecule	label	analyte	matrix	LOD	ref
aptamer-based lateral flow assay (LFA)	aptamer	Au NPs	*Mammaliicoccus* sp. RAM2 and *Pseudomonas* sp. RAC1	silkworm hemolymph	1.5×10^4; 1.5×10^3 CFU/mL	this study
immunochromatographic assay (ICA)	monoclonal antibodies	Au NPs	*Pseudomonas aeruginosa*	water and food samples	2.41×10^4 CFU/mL	54
aptamer-based lateral flow assay (LFA)	aptamer	Au NPs	*Salmonellatyphimurium*, *Escherichia coli* O157:H7, *Staphylococcus aureus*	food samples	5×10^3; 3×10^4; 2×10^4 CFU/mL	32
multiple loop-mediated isothermal amplification (mLAMP)-lateral flow nucleic acid biosensor (LFNAB)	antibody	Au NPs	*Pseudomonas aeruginosa*		20 CFU/mL	55
recombinase polymerase amplification (RPA) combined with lateral flow strip (LFS)	DNA primer		*Pseudomonas aeruginosa*	human wound exudate	2.1×10^5 CFU/mL	56
colorimetric detection	aptamer	Au NPs	*Staphylococcus aureus*	laboratory samples	1.5×10^7 cells/mL	57
colorimetric detection	aptamer	Au NPs	*Pseudomonas aeruginosa*	laboratory samples	10^5 CFU/mL	58
chemiluminescent detection	antibody	horseradish peroxidase	*Staphylococcus aureus*	spiked urine, apple juice, and glucose injection samples	6 CFU/mL	59
electrochemical detection	bacteriophage		*Staphylococcus aureus* MRSA USA300	clinical samples	1.29×10^2 CFU/mL	60
surface enhanced Raman spectroscopy aptasensor	aptamer	Au NPs	*Salmonella typhimurium*, *Staphylococcus aureus*	food samples	35 CFU/mL	61

specific strip showed positive results only for *Pseudomonas aeruginosa* MCC 2080, and the *Mammaliicoccus* sp. (formerly present under the *Staphylococcus* genus[31]) specific strip showed positivity only for *Staphylococcus aureus* MCC 2408. Every other tested bacterial species that were examined showed negative results (Figure 7b). It can be concluded that the LFA test strip biosensor exhibits a high degree of specificity toward their respective targets and thus can be used for real-time on-site sample analysis.

Real-Time On-Site Detection of Pathogens of Infected Silkworm. Aptamers offer a cost-effective and selective alternative to antibodies. Despite substantial progress in the development and design of aptamer-based lateral flow tests in recent years, none have been commercialized. To tackle this bottleneck and to explore the feasibility of the aptamer-based lateral flow test strip, we evaluated 20 infected silkworm hemolymph samples employing this approach. Our findings were consistent with earlier reports achieved using standard methods, indicating that our technology is suitable for real-time on-site detection of infected silkworms (Figure 7c). Furthermore, unlike existing conventional approaches, which are complex and time-consuming, our method is simple, rapid, cost-effective, and capable of detecting the desired targets with high specificity.

Colorimetric Assay. To validate our LFA-based detection, we also performed a colorimetric assay. The changes in color of the solution from red to blue and the UV−vis spectra showed that colorimetric assay-based detection was confirmed. This technique can detect *Pseudomonas* sp. RAC1 and *Mammaliicoccus* sp. RAM2 at concentrations of 1.5×10^3 and 1.5×10^4 CFU/mL, respectively. The sample remained red (Figure 8a,b; red, green, pink, and black curves) in the

https://doi.org/10.1021/acsabm.4c00833
ACS Appl. Bio Mater. 2024, 7, 5740−5753

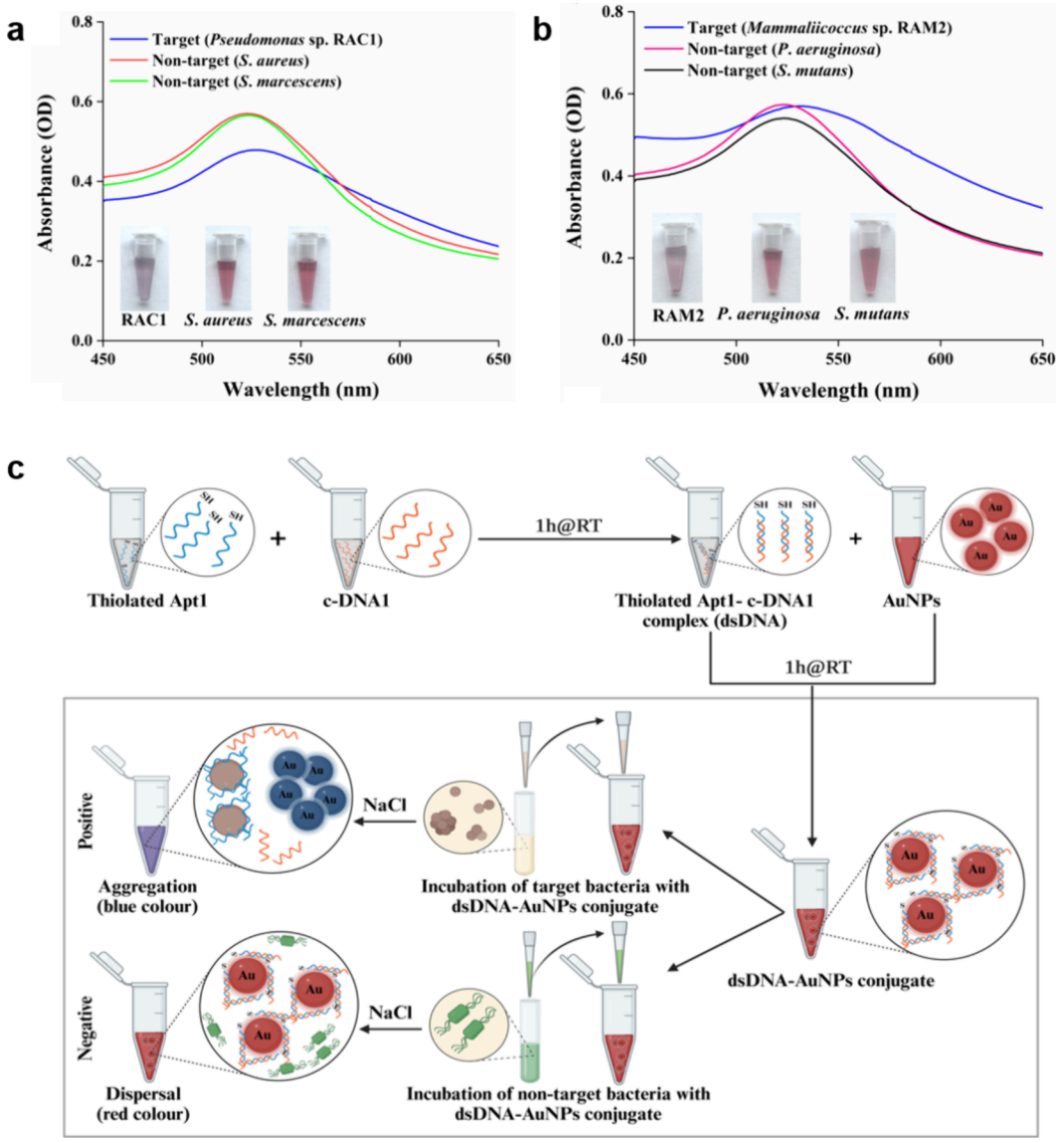

Figure 8. Absorbance spectra of the colorimetric assay for the specific detection of (a) *Pseudomonas* sp. RAC1 and (b) *Mammaliicoccus* sp. RAM2 in the presence of other bacteria. (c) Schematic representation of colorimetric bacterial detection.

absence of target bacteria following the addition of salt, while a blue color was observed (Figure 8a,b; blue curves) upon the addition of salt to the sample in the presence of target bacteria. UV−vis spectra showed changes in the absorbance, indicating the aggregation of Au NPs and aptamer binding with the target. The mechanism for the colorimetric detection of *Pseudomonas* sp. RAC1 and *Mammaliicoccus* sp. RAM2 was based on the deaggregation of Au NPs (Figure 8c). After the addition of salt, the solution remained red in the absence of the target. The prevention of salt-induced aggregation of Au NPs was linked to the presence of a dsDNA structure on the surface of Au NPs. However, in the presence of the target, the aptamers experience a decrease in affinity for Au NPs and detach from their surface. Subsequently, the Au NPs undergo aggregation as a result of the introduction of salt, leading to a change in the solution color from reddish to blue, confirming the aptamer-target complex formation.[62,63]

CONCLUSIONS

We successfully developed a detection platform for rapid identification of silkworm pathogenic bacteria with high specificity. Our first approach was the analysis of *Pseudomonas* sp. RAC1 and *Mammaliicoccus* sp. RAM2 through an aptamer-based lateral flow test strip. The developed LFAs produced results in minutes and were visually assessed by noticing the changes in a red color band in the test line. Moreover, the LFA platform was successfully applied for the detection of pathogenic bacteria in infected *Bombyx mori* L. hemolymph samples. The second methodological approach involved the utilization of an adsorption−desorption aptasensor for colorimetric bacterial detection employing Au NPs. The selectivity of these assays against other silkworm pathogens was documented. Thus, the platform delivers strong potential for future use as a reliable real-time on-site portable biosensor device. Until now, as per our knowledge, there are no dedicated commercially available dual aptamer-functionalized Au NPs-based LFA kits specific for the silkworm pathogenic bacteria. Future work should focus on the simultaneous

https://doi.org/10.1021/acsabm.4c00833
ACS Appl. Bio Mater. 2024, 7, 5740−5753

detection of multiple pathogens through aptamer−Au NPs-based LFA formats which may revolutionize sericulture industries or silk farmers in managing silk crop loss, along with providing knowledge on framing MDR pathogen-associated risk management policies in sericulture practice.

AUTHOR INFORMATION

Corresponding Authors

Yavuz Nuri Ertas − *Department of Biomedical Engineering and ERNAM-Nanotechnology Research and Application Center, Erciyes University, Kayseri 38039, Turkey; Department of Technical Sciences, Western Caspian University, Baku AZ1001, Azerbaijan;* orcid.org/0000-0002-6791-7484; Email: yavuznuri@gmail.com

Amit Kumar Mandal − *Department of Sericulture and Center for Nanotechnology Sciences (CeNS), Raiganj University, Raiganj, West Bengal 733134, India;* orcid.org/0000-0001-9249-5052; Email: amitmandal08@gmail.com

Authors

Rittick Mondal − *Department of Sericulture, Raiganj University, Raiganj, West Bengal 733134, India*

Joydeep Chakraborty − *Department of Microbiology, Raiganj University, Raiganj, West Bengal 733134, India;* orcid.org/0000-0002-6699-4074

Paulami Dam − *Department of Sericulture, Raiganj University, Raiganj, West Bengal 733134, India*

Shubhajit Shaw − *Department of Sericulture, Raiganj University, Raiganj, West Bengal 733134, India*

Debnirmalya Gangopadhyay − *Department of Sericulture, Raiganj University, Raiganj, West Bengal 733134, India*

Complete contact information is available at: https://pubs.acs.org/10.1021/acsabm.4c00833

Notes

The authors declare no competing financial interest.

ACKNOWLEDGMENTS

R.M. would like to acknowledge the Department of Science and Technology, Government of India, for the DST-INSPIRE Ph.D. Fellowship (DST-INSPIRE-SRF; INSPIRE Code-IF190457). A.K.M. acknowledges DST-SERB India for financial assistance (sanction order number: EEQ/2021/000058).

REFERENCES

(1) Sun, Z.; Lu, Y.; Zhang, H.; Kumar, D.; Liu, B.; Gong, Y.; Zhu, M.; Zhu, L.; Liang, Z.; Kuang, S.; Chen, F.; Hu, X.; Cao, G.; Xue, R.; Gong, C. Effects of BmCPV Infection on Silkworm Bombyx Mori Intestinal Bacteria. *PLoS One* **2016**, *11* (1), No. e0146313.

(2) Hosokawa, T.; Fukatsu, T. Relevance of Microbial Symbiosis to Insect Behavior. *Current Opinion in Insect Science* **2020**, *39*, 91−100.

(3) Nesa, J.; Sadat, A.; Buccini, D. F.; Kati, A.; Mandal, A. K.; Franco, O. L. Antimicrobial Peptides from *Bombyx Mori*: A Splendid Immune Defense Response in Silkworms. *RSC Adv.* **2020**, *10* (1), 512−523.

(4) Tayal, M. K.; Chauhan, T. P. S. Silkworm Diseases and Pests. In *Industrial Entomology*; Omkar, Ed.; Springer Singapore: Singapore, 2017; pp 265−289.

(5) Naskar, D.; Barua, R. R.; Ghosh, A. K.; Kundu, S. C. Introduction to Silk Biomaterials. In *Silk biomaterials for tissue engineering and regenerative medicine*; Elsevier, 2014; pp 3−40.

(6) Marzoli, F.; Antonelli, P.; Saviane, A.; Tassoni, L.; Cappellozza, S.; Belluco, S. Bombyx Mori from a Food Safety Perspective: A Systematic Review. *Food Research International* **2022**, *160*, No. 111679.

(7) Li, G.; Xia, X.; Zhao, S.; Shi, M.; Liu, F.; Zhu, Y. The Physiological and Toxicological Effects of Antibiotics on an Interspecies Insect Model. *Chemosphere* **2020**, *248*, No. 126019.

(8) Mondal, R.; Shaw, S.; Mandal, P.; Dam, P.; Mandal, A. K. Recent Advances in the Biosensors Application for Reviving Infectious Disease Management in Silkworm Model: A New Way to Combat Microbial Pathogens. *Arch. Microbiol.* **2024**, *206* (5), 206.

(9) Deepika, I.; Ramesh, K. V.; Kumar, I.; Singh, A.; Debnath, R.; Dubey, H.; Shukla, P.; Ponnuvel, K. M.; Moorthy, S. M.; Subrahmanyam, G. Molecular Diagnostics in Sericulture: A Paradigm Shift towards Disease Diagnosis in Silkworms. *Entomologia Exp Applicata* **2024**, *172* (5), 372−382.

(10) Nyaruaba, R.; Hong, W.; Li, X.; Yang, H.; Wei, H. Long-Term Preservation of SARS-CoV-2 RNA in Silk for Downstream RT-PCR Tests. *Anal. Chem.* **2022**, *94* (10), 4522−4530.

(11) Sohrabi, H.; Majidi, M. R.; Fakhraei, M.; Jahanban-Esfahlan, A.; Hejazi, M.; Oroojalian, F.; Baradaran, B.; Tohidast, M.; Guardia, M. D. L.; Mokhtarzadeh, A. Lateral Flow Assays (LFA) for Detection of Pathogenic Bacteria: A Small Point-of-Care Platform for Diagnosis of Human Infectious Diseases. *Talanta* **2022**, *243*, No. 123330.

(12) Wang, Z.; Zhao, J.; Xu, X.; Guo, L.; Xu, L.; Sun, M.; Hu, S.; Kuang, H.; Xu, C.; Li, A. An Overview for the Nanoparticles-Based Quantitative Lateral Flow Assay. *Small Methods* **2022**, *6* (1), No. 2101143.

(13) Danthanarayana, A. N.; Brgoch, J.; Willson, R. C. Photoluminescent Molecules and Materials as Diagnostic Reporters in Lateral Flow Assays. *ACS Appl. Bio Mater.* **2022**, *5* (1), 82−96.

(14) Fernández-Lodeiro, C.; González-Cabaleiro, L.; Vázquez-Iglesias, L.; Serrano-Pertierra, E.; Bodelón, G.; Carrera, M.; Blanco-López, M. C.; Pérez-Juste, J.; Pastoriza-Santos, I. Au@Ag Core−Shell Nanoparticles for Colorimetric and Surface-Enhanced Raman-Scattering-Based Multiplex Competitive Lateral Flow Immunoassay for the Simultaneous Detection of Histamine and Parvalbumin in Fish. *ACS Appl. Nano Mater.* **2024**, *7* (1), 498−508.

(15) Xu, X.; Wang, Z.; Guo, L.; Xu, X.; Wu, A.; Kuang, H.; Sun, L.; Song, S.; Xu, C. Sensitive Lateral Flow Immunoassay for the Residues of Imidocarb in Milk and Beef Samples. *ACS Omega* **2021**, *6* (4), 2559−2569.

(16) Aleem, A.; Akhtar, B.; Muhammad, F.; Qureshi, A. S.; Rahman, S. Development of a Lateral-Flow Immunochromatographic Strip for the Detection of Oxytetracycline Residues in Biological Fluids. *ACS Omega* **2023**, *8* (39), 36237−36244.

(17) Lee, I.; Kwon, S.-J.; Heeger, P.; Dordick, J. S. Ultrasensitive ImmunoMag-CRISPR Lateral Flow Assay for Point-of-Care Testing of Urinary Biomarkers. *ACS Sens.* **2024**, *9* (1), 92−100.

(18) Joung, Y.; Kim, K.; Lee, S.; Chun, B.-S.; Lee, S.; Hwang, J.; Choi, S.; Kang, T.; Lee, M.-K.; Chen, L.; Choo, J. Rapid and Accurate On-Site Immunodiagnostics of Highly Contagious Severe Acute Respiratory Syndrome Coronavirus 2 Using Portable Surface-Enhanced Raman Scattering-Lateral Flow Assay Reader. *ACS Sens.* **2022**, *7* (11), 3470−3480.

(19) Sena-Torralba, A.; Álvarez-Diduk, R.; Parolo, C.; Piper, A.; Merkoçi, A. Toward Next Generation Lateral Flow Assays: Integration of Nanomaterials. *Chem. Rev.* **2022**, *122* (18), 14881−14910.

(20) Khelifa, L.; Hu, Y.; Jiang, N.; Yetisen, A. K. Lateral Flow Assays for Hormone Detection. *Lab Chip* **2022**, *22* (13), 2451−2475.

(21) Mohammadinejad, A.; Nooranian, S.; Kazemi Oskuee, R.; Mirzaei, S.; Aleyaghoob, G.; Zarrabi, A.; Selda Gunduz, E.; Nuri Ertas, Y.; Sheikh Beig Goharrizi, M. A. Development of Lateral Flow Assays for Rapid Detection of Troponin I: A Review. *Critical Reviews in Analytical Chemistry* **2022**, 1−15.

(22) Tripathi, A.; Bonilla-Cruz, J. Review on Healthcare Biosensing Nanomaterials. *ACS Appl. Nano Mater.* **2023**, *6* (7), 5042−5074.

(23) Sahu, S.; Roy, R.; Anand, R. Harnessing the Potential of Biological Recognition Elements for Water Pollution Monitoring. *ACS Sens.* **2022**, *7* (3), 704−715.

(24) Frigoli, M.; Lowdon, J. W.; Caldara, M.; Cleij, T. J.; Diliën, H.; Eersels, K.; Van Grinsven, B. Emerging Biomimetic Sensor Technologies for the Detection of Pathogenic Bacteria: A Commercial Viability Study. *ACS Omega* **2024**, *9* (22), 23155−23171.
(25) Chakraborty, B.; Das, S.; Gupta, A.; Xiong, Y.; T-V, V.; Kizer, M. E.; Duan, J.; Chandrasekaran, A. R.; Wang, X. Aptamers for Viral Detection and Inhibition. *ACS Infect. Dis.* **2022**, *8* (4), 667−692.
(26) Wen, K.; Chen, Y.; Meng, X.; Botros, S.; Dai, W.; Stojanovic, M. N.; Tomer, R.; Lin, Q. A Microfluidic Dual-Aptamer Sandwich Assay for Rapid and Cost-Effective Detection of Recombinant Proteins. *Microchemical Journal* **2023**, *188*, No. 108454.
(27) Wei, Z.; Luciano, K.; Xia, X. Catalytic Gold-Iridium Nanoparticles as Labels for Sensitive Colorimetric Lateral Flow Assay. *ACS Nano* **2022**, *16* (12), 21609−21617.
(28) Erturan, A. M.; Lulek, E.; Cuhadar, S. N.; Ertas, Y. N.; Durmaz, H. Highly-Sensitive Detection of 2,4-Dinitrotoluene Using Colloidal Gold Nanospheres. *Sensors and Actuators A: Physical* **2024**, *369*, No. 115091.
(29) Park, J. W.; Park, S. K.; Jeong, C. Y.; Kwon, H. G.; Lee, J. H.; Kang, S. K.; Kim, S.-W.; Kim, S.-R. Microbial Community Changes in Silkworms Suspected of Septicemia and Identification of Serratia Sp. *International Journal of Molecular Sciences* **2024**, *25* (7), 3957.
(30) Gençer, D.; Şalvarcı, H. B.; Ulaşlı, B.; Cengiz, F. C.; Demir, İ. Bacterial Diversity Associated with the Hatay Yellow Strain Silkworm (Bombyx Mori L.): Isolation, Identification and Characterization. *Mustafa Kemal Üniversitesi Tarım Bilimleri Dergisi* **2023**, *28* (3), 593−605.
(31) de Moura, G. S.; de Carvalho, E.; Sanchez, E. M. R.; Sellera, F. P.; Marques, M. F.; Heinemann, M. B.; De Vliegher, S.; Souza, F. N.; Mota, R. A. Emergence of Livestock-Associated Mammaliicoccus Sciuri ST71 Co-Harbouring mecA and mecC Genes in Brazil. *Vet. Microbiol.* **2023**, *283*, No. 109792.
(32) Lu, C.; Gao, X.; Chen, Y.; Ren, J.; Liu, C. Aptamer-Based Lateral Flow Test Strip for the Simultaneous Detection of *Salmonella Typhimurium*, *Escherichia Coli* O157:H7 and *Staphylococcus Aureus*. *Anal. Lett.* **2020**, *53* (4), 646−659.
(33) Soundy, J.; Day, D. Selection of DNA Aptamers Specific for Live Pseudomonas Aeruginosa. *PLoS One* **2017**, *12* (9), No. e0185385.
(34) Some, S.; Sarkar, B.; Biswas, K.; Jana, T. K.; Bhattacharjya, D.; Dam, P.; Mondal, R.; Kumar, A.; Deb, A. K.; Sadat, A.; Saha, S.; Kati, A.; Ocsoy, I.; Franco, O. L.; Mandal, A.; Mandal, S.; Mandal, A. K.; İnce, İ. A. Bio-Molecule Functionalized Rapid One-Pot Green Synthesis of Silver Nanoparticles and Their Efficacy toward the Multidrug Resistant (MDR) Gut Bacteria of Silkworms (Bombyx Mori). *RSC Adv.* **2020**, *10* (38), 22742−22757.
(35) Nesa, J.; Jana, S. K.; Sadat, A.; Biswas, K.; Kati, A.; Kaya, O.; Mondal, R.; Dam, P.; Thakur, M.; Kumar, A.; Hossain, M.; Lima, L. R.; Rezende, S. B.; Bhattacharjya, D.; Gangopadhyay, D.; Ghorai, S.; Altuntas, S.; Panda, A. K.; Chakrabarti, P.; Swarnakar, S.; Chakraborty, J.; Yilmaz, B.; Macedo, M. L. R.; Franco, O. L.; Cardoso, M. H.; Mandal, A. K. Antimicrobial Potential of a Ponericin-like Peptide Isolated from Bombyx Mori L. Hemolymph in Response to Pseudomonas Aeruginosa Infection. *Sci. Rep.* **2022**, *12* (1), 15493.
(36) Rashidzadeh, H.; Seidi, F.; Ghaffarlou, M.; Salehiabar, M.; Charmi, J.; Yaray, K.; Nosrati, H.; Ertas, Y. N. Preparation of Alginate Coated Pt Nanoparticle for Radiosensitization of Breast Cancer Tumor. *Int. J. Biol. Macromol.* **2023**, *233*, No. 123273.
(37) Marmur, J. A Procedure for the Isolation of Deoxyribonucleic Acid from Micro-Organisms. *Journal of molecular biology* **1961**, *3* (2), 208−218.
(38) Some, S.; Bulut, O.; Biswas, K.; Kumar, A.; Roy, A.; Sen, I. K.; Mandal, A.; Franco, O. L.; İnce, İ. A.; Neog, K.; Das, S.; Pradhan, S.; Dutta, S.; Bhattacharjya, D.; Saha, S.; Mohapatra, P. K. D.; Bhuimali, A.; Unni, B. G.; Kati, A.; Mandal, A. K.; Yilmaz, M. D.; Ocsoy, I. Effect of Feed Supplementation with Biosynthesized Silver Nanoparticles Using Leaf Extract of Morus Indica L. V1 on Bombyx Mori L.(Lepidoptera: Bombycidae). *Sci. Rep.* **2019**, *9* (1), 14839.
(39) Mondal, R.; Dam, P.; Chakraborty, J.; Shaw, S.; Pradhan, S.; Das, S.; Nesa, J.; Meena, K.; Ghati, A.; Chaudhuri, S. D.; Bhattacharjee, D.; Mandal, V.; Sarkar, B.; Mandal, A. K. Genomic Dataset of a Multiple-Drug Resistant Pseudomonas Sp. Strain RAC1 Isolated from a Flacherie Infected Nistari Race of Bombyx Mori L. *Data Brief.* **2024**, *54*, No. 110293.
(40) Mao, D.-P.; Zhou, Q.; Chen, C.-Y.; Quan, Z.-X. Coverage Evaluation of Universal Bacterial Primers Using the Metagenomic Datasets. *BMC Microbiol* **2012**, *12* (1), 66.
(41) Minerdi, D.; Fani, R.; Gallo, R.; Boarino, A.; Bonfante, P. Nitrogen Fixation Genes in an Endosymbiotic *Burkholderia* Strain. *Appl. Environ. Microbiol.* **2001**, *67* (2), 725−732.
(42) Dalirirad, S.; Steckl, A. J. Lateral Flow Assay Using Aptamer-Based Sensing for on-Site Detection of Dopamine in Urine. *Analytical biochemistry* **2020**, *596*, No. 113637.
(43) Boruah, J. S.; Devi, C.; Hazarika, U.; Reddy, P. V. B.; Chowdhury, D.; Barthakur, M.; Kalita, P. Green Synthesis of Gold Nanoparticles Using an Antiepileptic Plant Extract: In Vitro Biological and Photo-Catalytic Activities. *RSC Adv.* **2021**, *11* (45), 28029−28041.
(44) El-Borady, O. M.; Fawzy, M.; Hosny, M. Antioxidant, Anticancer and Enhanced Photocatalytic Potentials of Gold Nanoparticles Biosynthesized by Common Reed Leaf Extract. *Appl. Nanosci* **2023**, *13* (5), 3149−3160.
(45) Li, Y.; Baeta, C.; Aras, O.; Daniel, M.-C. Preparation of Lisinopril-Capped Gold Nanoparticles for Molecular Imaging of Angiotensin-Converting Enzyme. In *Smart Biomedical and Physiological Sensor Technology VI*; SPIE, 2009; vol *7313*, pp 9−16.
(46) Bu, L.; Yang, W.; Ming, H. Low Temperature Synthesis of Rutile TiO 2 Single Crystal Nanorods with Exposed (002) Facets and Their Decoration with Gold Nanoparticles for Photocatalytic Applications. *RSC Adv.* **2015**, *5* (56), 45122−45128.
(47) Hosny, M.; Eltaweil, A. S.; Mostafa, M.; El-Badry, Y. A.; Hussein, E. E.; Omer, A. M.; Fawzy, M. Facile Synthesis of Gold Nanoparticles for Anticancer, Antioxidant Applications, and Photocatalytic Degradation of Toxic Organic Pollutants. *ACS Omega* **2022**, *7* (3), 3121−3133.
(48) Quadir, S.; Khan, N. A.; Singh, D. K.; Faraz, A.; Jhingan, G. D.; Joshi, M. C. Exposure to High Dosage of Gold Nanoparticles Accelerates Growth Rate by Modulating Ribosomal Protein Expression. *ACS Nano* **2023**, *17* (16), 15529−15541.
(49) Nosrati, H.; Salehiabar, M.; Charmi, J.; Yaray, K.; Ghaffarlou, M.; Balcioglu, E.; Ertas, Y. N. Enhanced In Vivo Radiotherapy of Breast Cancer Using Gadolinium Oxide and Gold Hybrid Nanoparticles. *ACS Appl. Bio Mater.* **2023**, *6* (2), 784−792.
(50) Yaray, K.; Rashidzadeh, H.; Mozafari, F.; Rezaeejam, H.; Moghaddam, Z. K.; Ertas, Y. N.; Danafar, H. CuFe2O4 Decorated with BSA as a Potential Nanoradioenhancer for Enhanced X-Ray Radiation Therapy of Brain Tumor. *Chem. Pap.* **2023**, *77* (11), 7187−7196.
(51) Ekram, B.; Tolba, E.; El-Sayed, A. F.; Müller, W. E.; Schröder, H. C.; Wang, X.; Abdel-Hady, B. M. Cell Migration, DNA Fragmentation and Antibacterial Properties of Novel Silver Doped Calcium Polyphosphate Nanoparticles. *Sci. Rep.* **2024**, *14* (1), 565.
(52) Ligozzi, M.; Bernini, C.; Bonora, M. G.; De Fatima, M.; Zuliani, J.; Fontana, R. Evaluation of the VITEK 2 System for Identification and Antimicrobial Susceptibility Testing of Medically Relevant Gram-Positive Cocci. *J. Clin Microbiol* **2002**, *40* (5), 1681−1686.
(53) Khongwichit, S.; Swangphon, P.; Nanakorn, N.; Nualla-ong, A.; Choowongkomon, K.; Lieberzeit, P. A.; Chunta, S. A Simple Aptamer/Gold Nanoparticle Aggregation-Based Colorimetric Assay for Oxidized Low-Density Lipoprotein Determination. *Talanta* **2023**, *254*, No. 124199.
(54) Zeng, L.; Guo, L.; Wang, Z.; Xu, X.; Ding, H.; Song, S.; Xu, L.; Kuang, H.; Xu, C. Gold Nanoparticle-Based Immunochromatographic Assay for Detection Pseudomonas Aeruginosa in Water and Food Samples. *Food chemistry: X* **2021**, *9*, No. 100117.
(55) Chen, Y.; Cheng, N.; Xu, Y.; Huang, K.; Luo, Y.; Xu, W. Point-of-Care and Visual Detection of P. Aeruginosa and Its Toxin Genes by

https://doi.org/10.1021/acsabm.4c00833
ACS Appl. Bio Mater. 2024, 7, 5740−5753

Multiple LAMP and Lateral Flow Nucleic Acid Biosensor. *Biosens. Bioelectron.* **2016**, *81*, 317−323.
(56) Brunauer, A.; Verboket, R. D.; Kainz, D. M.; von Stetten, F.; Frueh, S. M. Rapid Detection of Pathogens in Wound Exudate via Nucleic Acid Lateral Flow Immunoassay. *Biosensors* **2021**, *11* (3), 74.
(57) Lim, S. H.; Ryu, Y. C.; Hwang, B. H. Aptamer-Immobilized Gold Nanoparticles Enable Facile and On-Site Detection of Staphylococcus Aureus. *Biotechnol Bioproc E* **2021**, *26* (1), 107−113.
(58) Schmitz, F. R. W.; Cesca, K.; Valério, A.; De Oliveira, D.; Hotza, D. Colorimetric Detection of Pseudomonas Aeruginosa by Aptamer-Functionalized Gold Nanoparticles. *Appl. Microbiol. Biotechnol.* **2023**, *107* (1), 71−80.
(59) Xiong, J.; Wang, W.; Zhou, Y.; Kong, W.; Wang, Z.; Fu, Z. Ultra-Sensitive Chemiluminescent Detection of Staphylococcus Aureus Based on Competitive Binding of Staphylococcus Protein A-Modified Magnetic Beads to Immunoglobulin G. *Microchim Acta* **2016**, *183* (4), 1507−1512.
(60) Patel, D.; Zhou, Y.; Ramasamy, R. P. A Bacteriophage-Based Electrochemical Biosensor for Detection of Methicillin-Resistant Staphylococcus Aureus. *J. Electrochem. Soc.* **2021**, *168* (5), No. 057523.
(61) Zhang, H.; Ma, X.; Liu, Y.; Duan, N.; Wu, S.; Wang, Z.; Xu, B. Gold Nanoparticles Enhanced SERS Aptasensor for the Simultaneous Detection of Salmonella Typhimurium and Staphylococcus Aureus. *Biosens. Bioelectron.* **2015**, *74*, 872−877.
(62) Ganguly, K.; Patel, D. K.; Dutta, S. D.; Lim, K.-T. TEMPO-Cellulose Nanocrystal-Capped Gold Nanoparticles for Colorimetric Detection of Pathogenic DNA. *ACS Omega* **2021**, *6* (19), 12424−12431.
(63) Sen, A.; Sester, C.; Poulsen, H.; Hodgkiss, J. M. Accounting for Interaction Kinetics between Gold Nanoparticles and Aptamers Enables High-Performance Colorimetric Sensors. *ACS Appl. Mater. Interfaces* **2022**, *14* (29), 32813−32822.

https://doi.org/10.1021/acsabm.4c00833
ACS Appl. Bio Mater. 2024, 7, 5740−5753